IEEE Access
Multidisciplinary ⋮ Rapid Review ⋮ Open Access Journal

Date of publication xxxx 00, 0000, date of current version xxxx 00, 0000.

Digital Object Identifier 10.1109/ACCESS.2022.Doi Number

Robust Yaw Stability Control of Commercial Vehicles

Jae-Hoon Jeong[1], Baek-soon Kwon[2]

[1]The School of Software, Kunsan National University, Gunsan, 54150, Korea

[2] The School of Mechanical System Engineering, Kunsan National University, Gunsan 54150, Korea

Corresponding author: Baek-soon Kwon (e-mail: bskwon@kunsan.ac.kr).

This research was supported by the National Research Foundation of Korea (NRF) grant funded by the Korea government (MSIT) (2022R1G1A1008259), the Technology Innovation Program (or Industrial Strategic Technology Development Program - Development of Automotive Industry Technology) (1415181583, 1415181226) funded by the Ministry of Trade, Industry & Energy (MOTIE, Korea), and the Korea Basic Science Institute (National Research Facilities and Equipment Center) grant funded by the Ministry of Education (2023R1A6C101B042).

ABSTRACT This paper describes a robust yaw stability control for commercial vehicles. In the case of commercial vehicles, parameter variations are relatively large compared to passenger vehicles due to significant variations in load conditions. The parameter variations in commercial vehicles can cause performance deterioration of a yaw stability controller designed with nominal parameters. So, it is necessary to design a robust yaw stability controller to guarantee its performance against parameter variations. In this study, the range of changes in significant parameters affecting the cornering behavior of the vehicle was analyzed, and a stochastic distribution was assumed for the changes. The methods of stochastic root locus and parameter sensitivity reduction are adopted to design a robust yaw stability controller. Computer simulations have been conducted to evaluate the stability and robust performance of the proposed controller. The simulations show that the proposed robust yaw stability controller is effective against parameter variations in commercial vehicles.

INDEX TERMS Commercial Vehicle, Linear Quadratic Regulator, Stochastic Root Locus, Parameter Sensitivity, Yaw Stability Control.

Nomenclature

a_x, a_y	Longitudinal and lateral accelerations (m/s^2)
C_f, C_r	Cornering stiffness of front/rear wheel (N/rad)
F_x F_y, F_z	Longitudinal, lateral, and vertical tire forces (N)
ΔF_x	Desired braking force (N)
g	Gravitational constant (=9.81m/s^2)
h	The height of CG from the roll center (m)
h_s	The height of CG from the ground (m)
I_x, I_y, I_z	Roll, pitch, and yaw moments of inertia (kg·m^2)
J_c, J_r	Objective functions of conventional and robust LQR
K_c, K_r	Feedback gain of conventional and robust LQR
l_f, l_r	The distances from C.G. to front/rear axles (m)
l	The wheelbase (m)
m	Total mass (weight, kg)
m_s	Sprung mass (kg)
M_z	Control yaw moment (N·m)
P_b	Brake pressure (MPa)
t_w	Track width (m)
v_x ,v_y	Longitudinal and lateral velocities (m/s)
ω	Wheel angular velocity (rad/s)
β	Side-slip angle (rad)
γ	Yaw rate (rad/s)
ϕ	Roll angle (rad)
δ_f	Steering wheel angle (rad)
λ	Pole
μ	Tire-road friction coefficient
σ, ω	Real and imaginary parts of a pole
σ_{th}	Stability criteria

I. INTRODUCTION

Electronic stability control (ESC) uses computer-controlled independent braking to follow a driver's intentions in critical driving situations. ESC is expected to play an essential role in reducing accidents in commercial vehicles. About ten years ago, the National Highway Traffic Safety Administration (NHTSA) issued a new Federal Motor Vehicle Safety Standard No. 136 to require ESC on heavy tractors and buses with a gross vehicle weight rating of more than 11,793 kilograms (26,000 pounds). In 2014, NHTSA expected that about 33.9 percent of new truck tractors and 80 percent of new buses covered by this rule would be equipped with ESC. Moreover, NHTSA estimates that ESC could reduce the un-tripped rollover and loss-of-control (LOC) crashes by 25 to 32 percent [1]. To evaluate the effect of ESC on commercial vehicles, NHTSA

conducted the HILS (Hardware-in-the-loop Simulation) test with Meritor WABCO [2].

Since commercial vehicles are more likely to be involved in fatal accidents and have higher vulnerabilities, they require a suitable yaw stability control strategy. Several research have proposed yaw stability control for single-unit vehicles. Steering control [3, 4], yaw moment control [5-8, 12-14], and coordination of steering and individual braking [9, 10] for yaw stability have been proposed so far. Chen and Tomizuka [11] designed a lateral controller for heavy vehicles using integrated steering and braking with a multivariable back-stepping technique. The stability performance of a vehicle can be evaluated on the phase plane of the yaw rate and the body side slip angle. Sun et al. proposed a switching principle for alternating between direct yaw moment control for energy-efficiency and stability on the phase plane [12]. Hu et al. proposed a faster and more accurate method for estimation of the vehicle stability region on the phase plane and applied it to a map-based controllers to improve the vehicle stability [13]. However, these approaches have not taken the variation of parameters into account. Hu et al. analyzed zero dynamics behavior based on a nonlinear vehicle model and showed that input/output linearization techniques for only yaw rate tracking can make the vehicle unstable [14]. They proposed a linear combination of the yaw rate and the side slip angle as the control output. Moreover, their work also introduced an analysis of the robust controller gain against to the vehicle parameter variation.

Although parameter variation is one of the most representative characteristics of commercial vehicles, robust controllers against parameter variations have not yet been studied sufficiently. Ploechl et el. designed a robust yaw stability controller for trailers using a sliding mode algorithm [15]. Their work showed that the proposed controller is robust to mass variation of the towing car and the trailer's center of gravity (CG) height. However, the parameter variation of load was not considered in their work. Oncu et al. proposed a robust yaw stability controller for commercial vehicles [16]. The paper's focus is not a yaw moment control, but rather a steering control. In this work, the authors designed the robust controller for six uncertain cases. However, changes in these factors and variations in some vehicle parameters, such as mass, cornering stiffness, and center of gravity, can lead to performance deterioration of yaw stability controllers. Therefore, it is necessary to design a robust controller against parameter variations.

Yim and Park have proposed a design procedure for a robust controller with trajectory sensitivity minimization and a parameter sensitivity reduction scheme for rollover prevention [17, 18]. These works assume that the height of CG, vehicle speed, and cornering stiffness of the front and rear wheels are uncertain. Palkovics and El-Gindy have proposed a robust active unilateral brake control system by considering the sensitivity analysis [19]. This work demonstrates that there is a need for the consideration of parametric variation in the controller design process. Calise and Byrns Jr. proposed a linear quadratic (LQ) cost function to reduce parameter sensitivity which differs from the conventional linear quadratic regulator (LQR) [20].

Stochastic robustness of linear time-invariant control systems and stochastic root loci were introduced in [21, 22]. These papers considered the probability of exceeding the settling time, exceeding the control limit, and instability when designing a controller. However, regarding robustness, the shape of the stochastic root locus should be considered. In our previous work [23], a robust yaw stability controller for commercial vehicles was designed to take advantages of stochastic root loci and parameter sensitivity reduction. In [23], a robust LQR was suggested to guarantee stability, less parameter sensitivity, and small amount of control input.

The controller design methodology covered in this paper is not much different from our previous work. However, there still are some differences when it comes to analysis of the uncertain parameters of commercial vehicles. The vehicle parameters were assumed to be random variables following the Gaussian probability distribution to obtain stochastic root loci. The variable range was derived from driving simulations, showing a significant difference between buses and sedans. Moreover, the control performance of yaw stability was verified through various driving scenarios compared to the previous work. In particular, the robustness of the controller concerning representative parameter variation was quantitatively analyzed.

II. DYNAMIC CHARACTERISTICS OF COMMERCIAL VEHICLES

Commercial vehicles are more likely to have uncertain parameters than passenger vehicles considering their purpose of use, e.g., a bus may carry passengers, a truck may carry freight, etc. The uncertain parameters of commercial vehicles generate various dynamic characteristics. A reasonable parameter range can be determined considering the vehicle load capacity and the load condition. The vehicle parameters are assumed to be Gaussian random variables in the reasonable range of vehicle parameters.

For simple analysis of lateral dynamic characteristics of commercial vehicles, the 2-DOF bicycle model is adopted in this paper. Assuming that the vehicle parameters are uncorrelated random variables, stochastic root loci of the dynamic model equations are obtained by Monte Carlo evaluation.

A. Analysis of the parameters of commercial vehicles

To express the parameter uncertainty stochastically, the variance of uncertain parameters is more significant for

TABLE I
NOMINAL VEHICLE PARAMETERS

	Passenger Vehicle (Sedan)			Commercial Vehicle (Bus)		
	Min.	Nom.	Max.	Min.	Nom.	Max.
m_s	1653	1803	1953	6360	7860	9360
I_{xx}	614	667	721	7695	8789	9883
I_{yy}	2765	2893	3022	30782	37032	43282
I_{zz}	2765	2922	3080	30782	37876	44969
l_f	1.353	1.411	1.469	2.513	2.941	3.370
l_r	1.579	1.637	1.695	1.119	1.548	1.976
h	0.230	0.245	0.260	0.70	0.80	0.90
t_w	1.60	1.60	1.60	2.03	2.03	2.03
C_f	2.71×10^4	3.42×10^4	4.12×10^4	6.52×10^4	1.26×10^5	1.86×10^5
C_r	2.67×10^4	3.50×10^4	4.32×10^4	8.30×10^4	1.82×10^5	2.80×10^5

commercial vehicles than passenger vehicles. In this paper, a bus of weight 6,360 kg, given in Trucksim®, and a sedan of weight 1,653 kg, given in Carsim®, were taken as representative commercial and passenger vehicles, respectively. Table I provides the parameters of these vehicles.

In Table I, the minimum values of the parameters are obtained under the assumption that the vehicles are unloaded. The maximum values of m_s, I_{xx}, and h are obtained under the assumption that the vehicles are fully loaded. Assuming that half of the weight capacity is biased to the front and rear wheels, the maximum values of I_{yy}, I_{zz}, l_f, and l_r are obtained. The nominal values of the parameters are calculated as the median between the minimum and the maximum values. However, the ranges of the cornering stiffness, C_f and C_r, cannot be easily obtained. Hence, it is calculated from simulations for specific driving conditions.

The most important factors affecting the cornering stiffness are the mass m_s, the weight distribution l_f, and the tire-road friction coefficient. To check the effect of variation of these parameters on cornering stiffness, a simulation is performed with the ramp steering input of 18 deg/s at an initial speed of 70 km/h on the vehicle simulation package, TruckSim®. The ramp steering input is suitable for obtaining the cornering stiffness because it can induce continuous varied lateral acceleration. Figure 1 shows the lateral tire forces used in the simulation.

Figures 2-(a) and (b) provide the lateral tire forces corresponding to tire slip angle and m_s. The nominal, the minimum, and the maximum values of m_s were set to 7860, 6360, and 9360 kg, respectively, as given in Table I**,** under the condition where the other parameters are set to their nominal values. The cornering stiffness can be calculated easily from the lateral tire force and the tire slip angle. Figures 2-(a) and (b) show that the larger the vehicle mass, the higher the cornering stiffness. This simulation obtained the cornering stiffness C_f and C_r as 9.01×10^4 to 1.64×10^5 N/rad and 1.83×10^5 to 2.80×10^5 N/rad, respectively.

Figures 2-(c) and (d) show the lateral tire forces with respect to tire slip angle and l_f. These correlations assume that half of the maximum allowable weight (1500 kg) is evenly loaded on the front axle, the center of the wheelbase, and the rear axle, respectively. The other parameters are set to their nominal values. Figures 2-(c) and (d) show that the larger the value of l_f, the higher the cornering stiffness of the rear wheel. In this simulation, the variations of C_f and C_r were obtained as 9.10×10^4 to 1.69×10^5 N/rad and 1.77×10^5 to 2.65×10^5 N/rad, respectively.

Figures 2-(e) and (f) show the lateral tire forces with respect to tire slip angle and the tire-road friction coefficient μ. The values of μ are set to high (1.0), nominal (0.8), and low (0.6). The other parameters are set to their nominal values. Figures 2-(e) and (f) show that the cornering stiffness decreases as the tire slip angle exceeds about 0.06 rad for μ of 0.6. In this simulation, the variations of C_f and C_r were obtained as 7.43×10^4 to 1.26×10^5 N/rad and 1.53×10^5 to 2.63×10^5 N/rad, respectively.

Finally, the variation of cornering stiffness associated with slip angle, m_s, l_f, and μ can be obtained. For example, the smallest C_f is obtained from the unloaded vehicle at μ of 0.6. The largest C_f is obtained when the vehicle is half-loaded on the front axle at μ of 1.0. Similarly, the smallest C_r is obtained when the vehicle is half-loaded on the front axle at μ of 0.6. The largest C_r is obtained when the vehicle is fully loaded at μ of 1.0. Figures 2-(g) and (h) provide the results. The variations of C_f and C_r were obtained as 6.52×10^4 to 1.86×10^5 N/rad and 8.30×10^5 to 2.80×10^5 N/rad, respectively.

Probability distributions of uncertain parameters are assumed to be Gaussian, and their standard deviations are assumed to have a value of one-sixth of uncertain ranges. Figure 3 shows the overall ranges of uncertain parameters obtained by considering all the above scenarios.

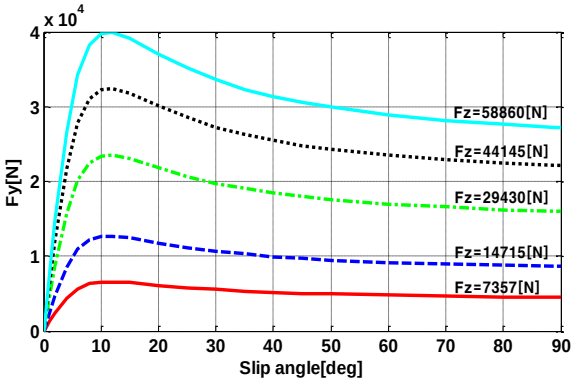

FIGURE 1. Lateral tire forces used in simulation.

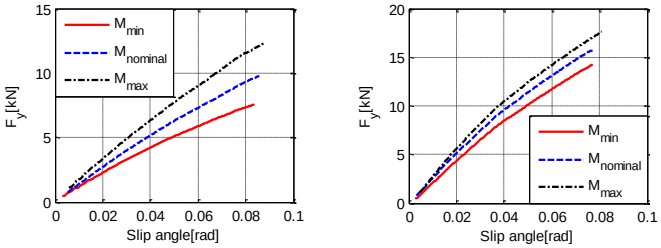

(a) Front tire (b) Rear tire

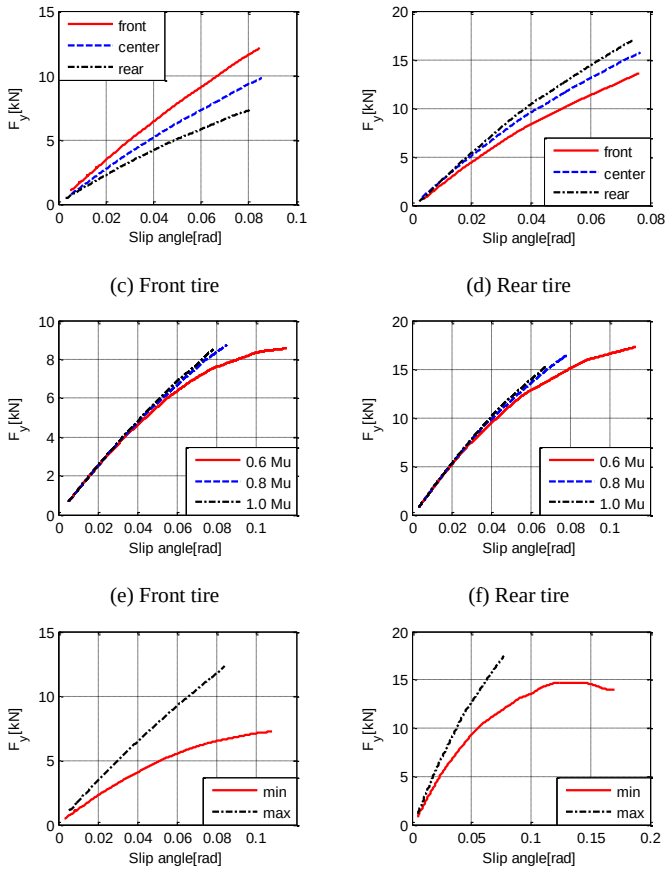

(c) Front tire (d) Rear tire

(e) Front tire (f) Rear tire

(g) Front tire (h) Rear tire

FIGURE 2. Lateral force curves of front and rear tire with respect to: sprung mass (a, b), the distances from C.G. to front axle (c, d), friction coefficient (e, f), and resulting min-max condition (g, h).

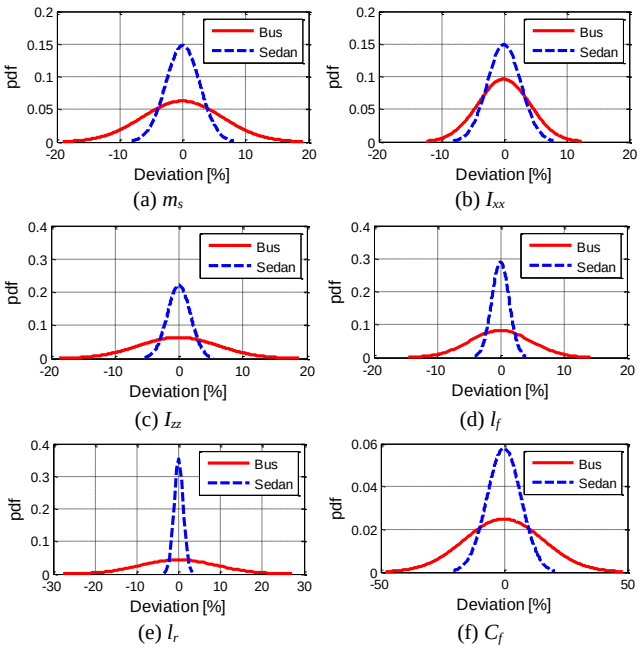

(a) m_s (b) I_{xx}

(c) I_{zz} (d) l_f

(e) l_r (f) C_f

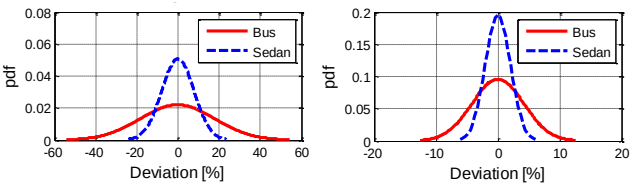

(g) C_r (h) h

FIGURE 3. Probability density functions of uncertain parameters for typical buses and sedans.

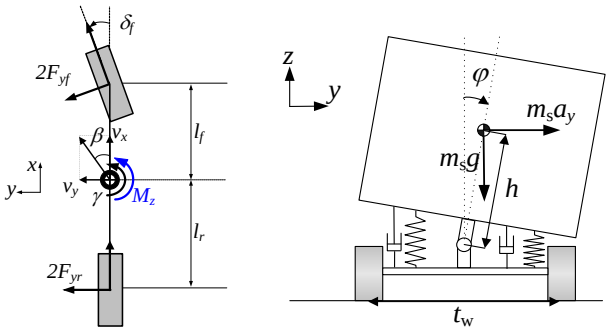

(a) 2-DOF bicycle model (b) 1-DOF roll model

FIGURE 4. 3-DOF vehicle model.

B. Lateral dynamics analysis of commercial vehicles

A 3-DOF vehicle model is used to build the equations of lateral, yaw, and roll motion, as given in (1), (2), and (3), respectively [17]. This model consists of a 2-DOF bicycle model and a 1-DOF roll model, as shown in Figure 4.

$$m v_x(\dot{\beta}+\gamma) - m_s h\ddot{\varphi} = F_{yf} + F_{yr} \tag{1}$$

$$I_{zz}\dot{\gamma} = l_f F_{yf} - l_r F_{yr} + M_z \tag{2}$$

$$I_{xx}\ddot{\varphi} = -K_\phi\varphi - C_\phi\dot{\varphi} + m_s h v_x(\dot{\beta}+\gamma) + m_s g h\varphi \tag{3}$$

Assuming that tire slip angles are within linear region, the lateral tire force F_{yf} and F_{yr} are given as (4).

$$F_{yf} = -C_f\alpha_f, \quad F_{yr} = -C_r\alpha_r \tag{4}$$

where

$$\alpha_f = \frac{v_y + l_f\gamma}{v_x} - \delta_f, \quad \alpha_r = \frac{v_y - l_r\gamma}{v_x}$$

The state vector $\mathbf{x}$, control input u, disturbance w, and uncertain vehicle parameters vector $\mathbf{v}$ are defined as follows:

$$\begin{aligned} \mathbf{x} &= \begin{bmatrix} \beta & \gamma & \varphi & \dot{\varphi} \end{bmatrix}^T \\ u &= M_z \\ w &= \delta_f \\ \mathbf{v} &= \begin{bmatrix} v_1 & v_2 & \cdots & v_p \end{bmatrix} = \begin{bmatrix} m_s, h, l_f, C_f, C_r, I_{xx}, I_{zz} \end{bmatrix} \end{aligned} \tag{5}$$

From these definitions and the equations of motion, the state-space equation of the vehicle model is obtained as follows:

$$\begin{aligned} \dot{\mathbf{x}}(\mathbf{v}) &= \mathbf{A}(\mathbf{v})\mathbf{x} + \mathbf{B}_1(\mathbf{v})w + \mathbf{B}_2(\mathbf{v})u \\ &= \mathbf{E}^{-1}\mathbf{A}_e\mathbf{x} + \mathbf{E}^{-1}\mathbf{B}_{e1}w + \mathbf{E}^{-1}\mathbf{B}_{e2}u \end{aligned} \tag{6}$$

where

$$\mathbf{E}=\begin{bmatrix} mv_x & 0 & 0 & -m_s h \\ 0 & I_{zz} & 0 & 0 \\ 0 & 0 & 1 & 0 \\ -m_s h v_x & 0 & 0 & I_{xx} \end{bmatrix},\quad \mathbf{B_{e1}}=\begin{bmatrix} 2C_f \\ 2l_f C_f \\ 0 \\ 0 \end{bmatrix}$$

$$\mathbf{A_e}=\begin{bmatrix} a_{11} & a_{12} & 0 & 0 \\ a_{21} & a_{22} & 0 & 0 \\ 0 & 0 & 0 & 1 \\ 0 & m_s h v_x & -K_\phi + m_s g h & -C_\varphi \end{bmatrix},\quad \mathbf{B_{e2}}=\begin{bmatrix} 0 \\ 1 \\ 0 \\ 0 \end{bmatrix}$$

where

$$a_{11}=-2\left(C_f+C_r\right),\quad a_{12}=-mv_x-\frac{2\left(l_f C_f-l_r C_r\right)}{v_x},$$

$$a_{21}=-2\left(l_f C_f-l_r C_r\right),\quad a_{22}=-\frac{2\left(l_f{}^2 C_f+l_r{}^2 C_r\right)}{v_x}$$

The eigenvalues of system matrix **A** depend on the uncertain parameters vector **v**. Suppose that the parameters, m_s, h, l_f, C_f, C_r, I_{xx}, and I_{zz} are Gaussian random variables. Their nominal values and standard deviations are specified in the preceding section. Assuming that all random variables are uncorrelated, the locations of roots will be closer to their nominal values. Figures 5-(a) and (b) describe the scatter plots of pole locations and note that the poles of a commercial vehicle are located more widely than those of a passenger vehicle because of the more significant variance of uncertain parameters. From a statistical perspective, these scatter plots can be transformed into stochastic root loci by applying root density. This is achieved through counting the number of roots on the subspaces of the *s*-plane with Monte Carlo evaluation. Figures 5-(c) and (d) plot the stochastic root loci of the characteristic equation of the matrix **A**. The most probable dominant poles of a passenger vehicle are located at (-6.5, 0) and (-5, ±2.5) on the *s*-plane, and those of a commercial vehicle are located at (-6.5, ±2) and (-2, 0)**.**

In the case of bus, unstable poles are observed, which implies the vehicle is in over-steering condition. A simulation was conducted to compare the yaw stability by adjusting the vehicle parameters to cause extreme oversteer. Figure 6 shows the yaw rate comparison for the change in load conditions, when the vehicle conduct double lane change with 72 kph at μ of 0.5. In Figure 6, nominal and severe load conditions means that half of the maximum allowable weight (1500 kg) is evenly loaded on the center of the wheelbase and the rear axle, respectively. It shows that yaw instability is caused by the rearward half loaded condition.

III. Design of Robust Yaw Stability Controller for Commercial Vehicles

A comparison between commercial and passenger vehicles demonstrates that the parameter uncertainty and the probability of instability are higher for commercial vehicles compared to passenger vehicles. Therefore, it is necessary to design a robust yaw stability controller to deal with parameter uncertainty in commercial vehicles. First, a 3-DO

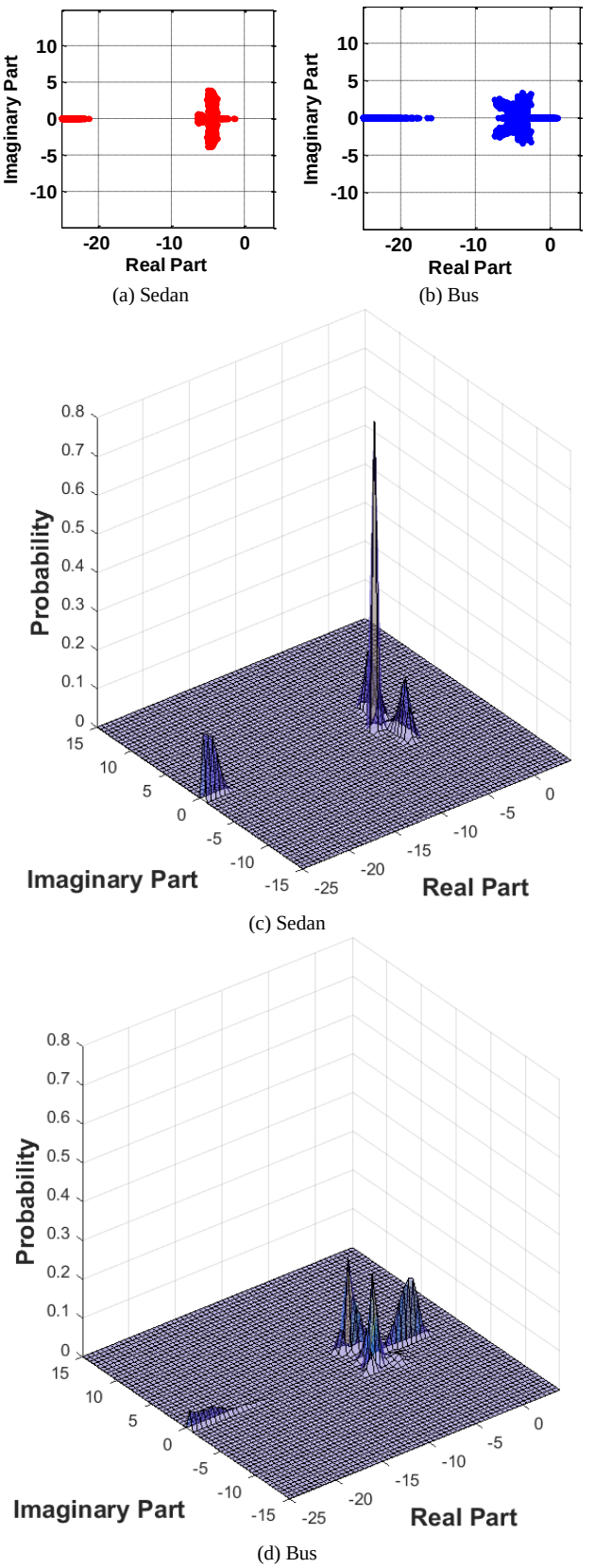

FIGURE 5. Scatter plots of pole locations and stochastic root loci for: sedan (a, c) and bus (b, d).

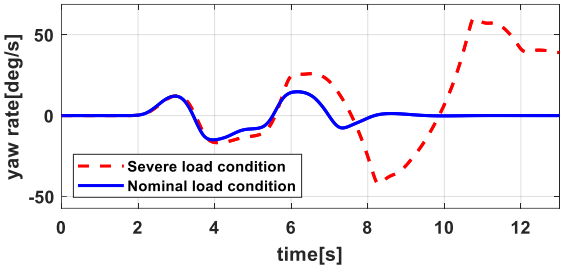

FIGURE 6. Yaw stability comparison according to load conditions during double lane change.

F vehicle with zero steering model is used to design the LQR. Then, the feedback gain of the LQR is determined to reduce parameter sensitivity.

A. Conventional controller design

The conventional LQR is designed in this section. Assuming that there are no disturbances, the control law of $u = -\mathbf{K}_c\mathbf{x}$ tries to minimize the following quadratic cost function.

$$\begin{aligned} J_c &= \int_0^\infty \left(q_{1,c}\beta^2 + q_{2,c}\gamma^2 + q_{3,c}\varphi^2 + q_{4,c}\dot{\varphi}^2 + r_c M_z{}^2\right)dt \\ &= \int_0^\infty \left(\mathbf{x}^T\mathbf{Q}_c\mathbf{x} + u^T\mathbf{R}_c u\right)dt \end{aligned} \tag{7}$$

where $\mathbf{Q}_c = diag[q_{1,c}, q_{2,c}, q_{3,c}, q_{4,c}]$, $\mathbf{R}_c = r_c$.

By solving the following Riccati equation, the feedback gain $\mathbf{K}_c$ can be easily computed as (8).

$$\mathbf{K}_c = \mathbf{R}_c^{-1}\mathbf{B}_{2,0}{}^T\mathbf{P}_c \tag{8}$$

where $\mathbf{A}_0^T\mathbf{P}_c + \mathbf{P}_c\mathbf{A}_0 - \mathbf{P}_c\mathbf{B}_{2,0}\mathbf{R}_c^{-1}\mathbf{B}_{2,0}^T\mathbf{P}_c + \mathbf{Q}_c = 0$

$\mathbf{A}_0$ and $\mathbf{B}_{2,0}$ are the system matrices with nominal vehicle parameters. As shown in Figure 5, the nominal values used to design the conventional parameters are not constant but uncertain. To deal with the uncertain parameter, it is necessary to design a controller for time-varying systems or an adaptive controller. However, the design procedure requires more expensive equipment and complexity, relatively. For this reason, a robust controller should be designed to cope with the parameter uncertainty.

B. Parameter sensitivity analysis of commercial vehicles

Uncertain parameters influence system matrices, $\mathbf{A}$, $\mathbf{B}_1$, and $\mathbf{B}_2$ in (6). By differentiating (6), the parameter sensitivity vector with respect to a particular parameter v_i at its nominal value $v_i{}^0$ can be obtained as (9).

$$\dot{\boldsymbol{\sigma}}_i = \mathbf{A}\left(\mathbf{v}_i^0\right)\boldsymbol{\sigma}_i + \left.\frac{\partial\mathbf{A}}{\partial v_i}\right|_{v_i=v_i^0}\mathbf{x} + \left.\frac{\partial\mathbf{B}_1}{\partial v_i}\right|_{v_i=v_i^0}w + \left.\frac{\partial\mathbf{B}_2}{\partial v_i}\right|_{v_i=v_i^0}u + \mathbf{B}_2\left(\mathbf{v}_i^0\right)\frac{\partial u}{\partial v_i} \tag{9}$$

where

$$\boldsymbol{\sigma}_i = \left.\frac{\partial\mathbf{x}}{\partial v_i}\right|_{v_i=v_i^0}$$

In (9), the subscript $v_i = v_i{}^0$ will be omitted hereinafter. The magnitudes of parameter sensitivity vectors can be obtained by using (9) when driving a vehicle. However, their absolute magnitudes are not suitable for analyzing the parameter sensitivity since the ranges of uncertain vehicle parameters are different. Therefore, multiplying each parameter sensitivity vector by respective standard deviations based on Figure 5 provides a more intuitive and reasonable analysis of probabilistic parameter sensitivity. This means:

$$\Delta\mathbf{x}_i = \left(\frac{\partial\mathbf{x}}{\partial v_i}\right)\Delta v_{i,std} \tag{10}$$

In (10), $\Delta\mathbf{x}_i$ indicates how much the *i-th* parameter variation affects the state trajectory. For instance, the parameter sensitivities for several uncertain parameters can be obtained during a double-lane change, as shown in Figure 7. In most situations, parameter sensitivity regarding front/rear cornering stiffness, C_f /C_r, and the distance from CG to front/rear axles, l_f, are more significant than other parameters. So, the normalized *i-th* parameter sensitivity can be defined as (11).

$$\left|\overline{\Delta\mathbf{x}_i}\right| = \frac{\max\left(\left|\Delta\mathbf{x}_i\right|\right)}{\sum_i \max\left(\left|\Delta\mathbf{x}_i\right|\right)} \tag{11}$$

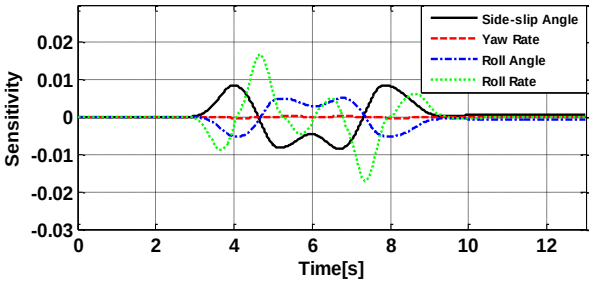

(a) m_s

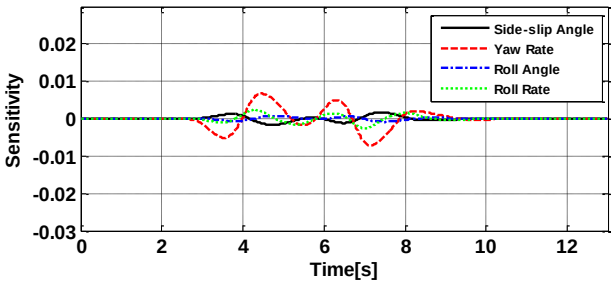

(b) I_{zz}

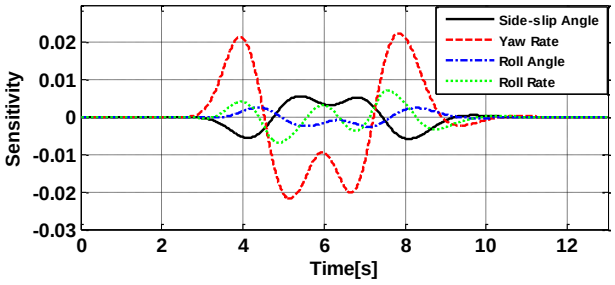

(c) l_f

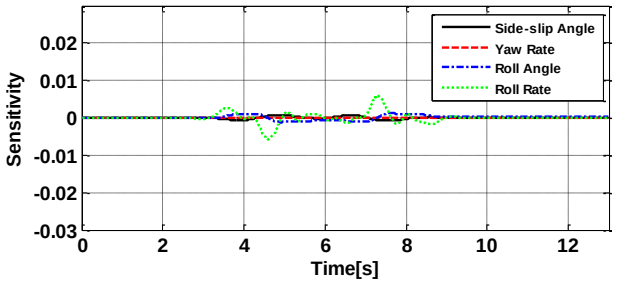

(d) I_{xx}

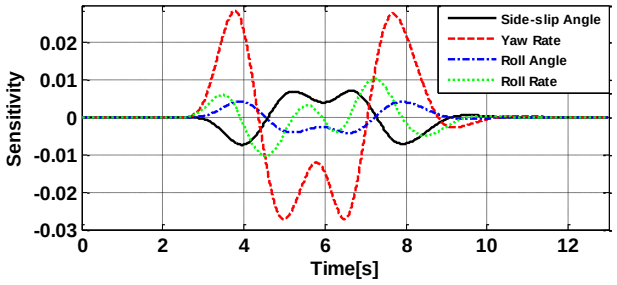

(e) C_f

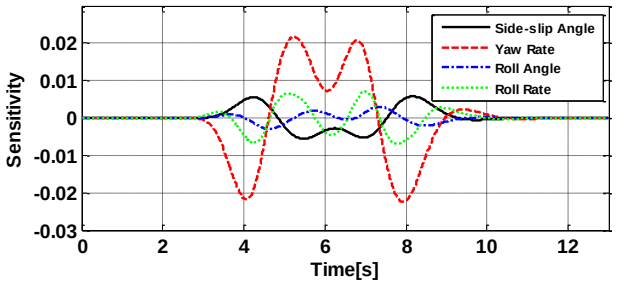

(f) C_r

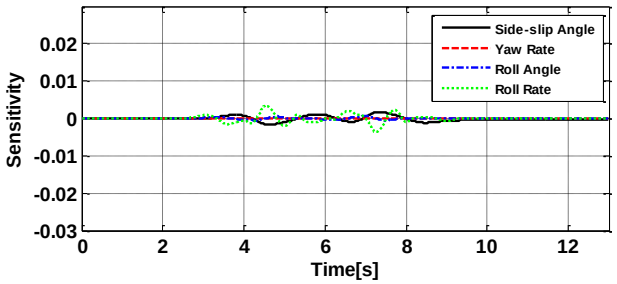

(g) h

FIGURE 7. Sensitivities of uncertain parameters for double lane change.

C. Robust controller design

In this section, the robust LQR is designed to reduce parameter sensitivity as proposed in the preceding section. (9) can be rewritten as (12), with the full-state feedback controller, u=–$\mathbf{K}_r\mathbf{x}$.

$$\dot{\boldsymbol{\sigma}}_{\mathbf{i}} = \mathbf{A}_c\boldsymbol{\sigma}_i + \mathbf{A}_{cs,i}\mathbf{x}, \quad i = 1,\cdots,p \tag{12}$$

where $\mathbf{A}_c \equiv (\mathbf{A}-\mathbf{B}_2\mathbf{K}_r), \mathbf{A}_{cs,i} \equiv \left(\frac{\partial \mathbf{A}}{\partial v_i} - \frac{\partial \mathbf{B}_2}{\partial v_i}\mathbf{K}_r\right)$.

Since the first term on the right-hand side is stabilized by feedback control, the last term should be reduced to guarantee the insensitivity against the variation of uncertain parameters. LQ cost function for parameter sensitivity reduction can be expressed as (13) by using (12) [20].

$$J_r = \int_0^\infty \{\mathbf{x}^T\left[\mathbf{Q}_r + \sum_i \rho_i \mathbf{A}_{cs,i}^T\mathbf{A}_{cs,i}\right]\mathbf{x} + u^T\mathbf{R}_r u\}dt \tag{13}$$

where $\mathbf{Q}_r = diag[q_{1,r}, q_{2,r}, q_{3,r}, q_{4,r}]$, $\mathbf{R}_r = r_r$.

The subscript i in (13) represents the uncertain parameters given in (5). A size of weighting factor ρ_i is determined by considering the normalized i-th parameter sensitivity based on (11) and the variance as (14).

$$\rho_i = \left|\overline{\Delta \mathbf{x}_i}\right| \cdot \left(\Delta v_{i,std}\right)^2 \tag{14}$$

For arbitrary $\mathbf{Q}_r$ and $\mathbf{R}_r$ matrices, the optimal feedback gain can be obtained as (15). We can obtain $\mathbf{K}_r$ by solving (15) numerically using the gradient method [24].

$$\begin{aligned} &\mathbf{K}_r = \mathbf{R}_r^{-1}\mathbf{B}_2{}^T\mathbf{P}_r \\ &\mathbf{A}^T\mathbf{P}_r + \mathbf{P}_r\mathbf{A} - \mathbf{P}_r\mathbf{B}_2\mathbf{R}_r^{-1}\mathbf{B}_2{}^T\mathbf{P}_r + \mathbf{Q}_r + \sum_i \rho_i \mathbf{A}_{cs,i}^T\mathbf{A}_{cs,i} = 0 \end{aligned} \tag{15}$$

With computed $\mathbf{K}_r$, two probabilities of stability and robustness of the closed-loop system are defined and computed by Monte Carlo evaluation, as given in (16).

$$\begin{aligned} &P_{A,1} = \int_Q I_1\left[P(\mathbf{v}), C(\mathbf{d})\right] pr(q)\,dq \\ &where, I_1 = \begin{cases} 1, \text{if } real(\lambda) > \sigma_{th} \\ 0, \text{otherwise} \end{cases} \\ &P_{B,1} = \int\int I_2\left[pr(\lambda)\right] d\sigma d\omega \\ &where, I_2 = \begin{cases} 1, \text{if } pr(\lambda) \neq 0 \\ 0, \text{otherwise} \end{cases} \end{aligned} \tag{16}$$

$P_{A,1}$ is the probability of real parts of pole locations, being larger than certain value σ_{th}, and $P_{B,1}$ is the projected area on the s-plane of stochastic root locus with respect to the system model of (6). **d** in (16) is the design parameter vector. In this paper, we define **d** as (17).

$$\mathbf{d} = \left[q_{1,r}, q_{2,r}, q_{3,r}, q_{4,r}, r_r, \rho_i\right] \tag{17}$$

We define the overall cost function as the sum of $P_{A,1}$ and $P_{B,1}$, with the weightings $w_{A,1}$ and $w_{B,1}$ as (18).

$$J = w_{A,1}P_{A,1} + w_{B,1}P_{B,1} \tag{18}$$

$P_{A,1}$ is directly related to the degree of stability. $P_{B,1}$ represents the robustness since the system's response is insensitive to parameter uncertainty if $P_{B,1}$ is low. Therefore, if one wants to guarantee the high degree of stability, $w_{A,1}$ should be set larger than $w_{B,1}$. Conversely, setting $w_{B,1}$ larger than $w_{A,1}$ can focus on robustness. For different values of the design parameters, it is necessary to find the optimum to minimize (18), to obtain the satisfactory level of stability and the robustness in the sense of the stochastic root locus. Figure 8 depicts the overall control design procedure as a flow chart. Figures 9-(a) and (b) show the scatter plots of dominant pole locations for commercial vehicle model with conventional and robust LQR controllers. The unknown parameter statistics, nominal value, and variation are formulated in Monte Carlo running, as analyzed in section II.

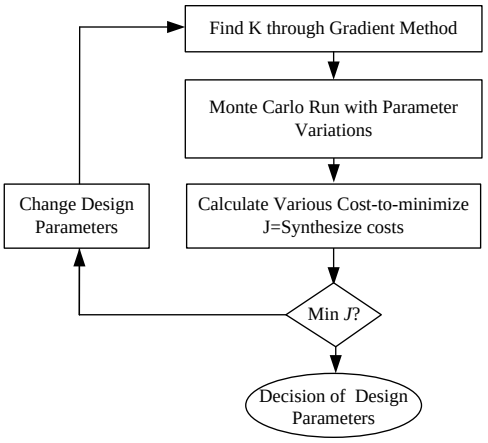

FIGURE 8. Design procedure of the robust controller.

Compared with the scatter plot of pole locations for the uncontrolled system in Figure 5-(b), the two controlled systems have no unstable poles, whereas the uncontrolled system has unstable poles. The proximate pole to the $j\omega$-axis of the robust LQR system is located at (-1.47, 0) on the s-plane, whereas that of the conventional LQR is located at (-0.18, 0). This means the robust LQR controller makes the system more stable than the conventional one in the worst case. Stochastic root loci of two controlled systems are shown in Figures 9-(c) and (d). The most probable dominant poles of conventional LQR system are located at (-6, 0), (-3, 0) on the s-plane, and those of robust LQR system are located at (-6, 0), (-4, 0). In the conventional LQR system, the probability that poles are distributed in unit circles centering

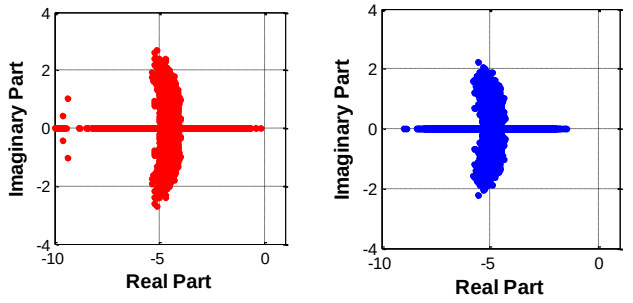

(a) Conventional LQR (b) Robust LQR

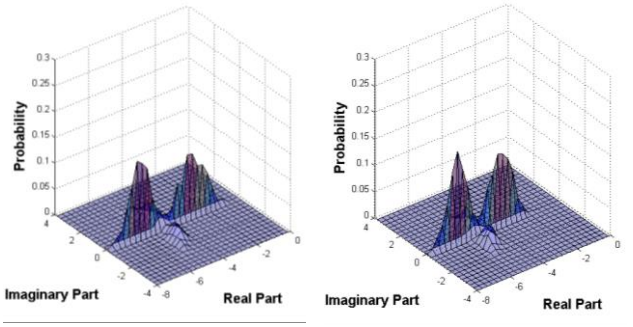

(c) Conventional LQR (d) Robust LQR

FIGURE 9. Scatter plots of dominant pole locations of controlled system and stochastic root loci nearby jω-axis for: conventional LQR (a, c) and robust LQR (b, d)

the dominant poles is 0.26. In the case of the robust LQR system, the probability is 0.29. The system with a robust LQR controller has more compact dominant poles, guaranteeing robust yaw stability performance against the parameter variation. In conclusion, the conventional LQR controller, with the nominal parameter used to design, would only guarantee the control performance under the nominal case. On the other hand, in the design procedure of the robust LQR controller, the reduction of parameter sensitivity of the state trajectory was considered so that the robust LQR controller could have enhanced control performance than the conventional LQR controller when the parameters are not nominal values.

D. Tire force distribution for yaw stability control

In this paper, a 3-DOF vehicle model with a commercial vehicle's nominal parameters is used to compute the target vehicle response. A target vehicle dynamic response, which is the desired yaw rate and body slip angle for a driver's steering input, is defined as follows [25]:

$$\gamma_d = \frac{\gamma_{ss,n}}{1+\tau_1 s}\cdot\delta_f, \quad \beta_d = \frac{\beta_{ss,n}}{1+\tau_2 s}\cdot\delta_f \tag{19}$$

where

$$\gamma_{ss,n} = \frac{2C_{f,n}C_{r,n}lv_x}{2C_{f,n}C_{r,n}l^2 - m_n v_x^2(l_{f,n}C_{f,n} - l_{r,n}C_{r,n})}$$

$$\beta_{ss,n} = \frac{2C_{f,n}C_{r,n}l_{r,n}l - m_n C_{f,n}l_{f,n}v_x^2}{2C_{f,n}C_{r,n}l^2 - m_n v_x^2(l_{f,n}C_{f,n} - l_{r,n}C_{r,n})}$$

τ_1 and τ_2 are time constants. Subscript n means nominal parameter and the subscript ss means steady state. The desired roll angle corresponding to the desired yaw rate is given as follows:

$$\varphi_d = \frac{\varphi_{ss,n}}{1+\tau_3 s}\cdot\gamma_d \tag{20}$$

where

$$\varphi_{ss,n} = \frac{m_{s,n}h_n v_x}{K_\varphi - m_{s,n}gh_n}$$

and τ_3 is a time constant. The state space model of the desired vehicle dynamics is given as follows:

$$\dot{\mathbf{x}}_d = \mathbf{A}_d\mathbf{x}_d + \mathbf{B}_d\delta_f$$

$$\mathbf{A}_d = \begin{bmatrix} -\frac{1}{\tau_1} & 0 & 0 & 0 \\ 0 & -\frac{1}{\tau_1} & 0 & 0 \\ 0 & 0 & 0 & 1 \\ 0 & 0 & -\frac{1}{\tau_1\tau_2} & -\frac{(\tau_1+\tau_2)}{\tau_1\tau_2} \end{bmatrix}, \quad \mathbf{B}_d = \begin{bmatrix} \frac{\beta_{ss}}{\tau_1} \\ \frac{\gamma_{ss}}{\tau_1} \\ 0 \\ \frac{\gamma_{ss}\varphi_{ss}}{\tau_1\tau_2} \end{bmatrix} \tag{21}$$

where

$$\mathbf{x}_d = \begin{bmatrix} \beta_d & \gamma_d & \varphi_d & \dot{\varphi}_d \end{bmatrix}^T$$

A yaw stability controller is designed based on model matching technique [26]. Let's define the error signal vector as $\mathbf{e} = \mathbf{x} - \mathbf{x}_d$. Then, the error dynamics can be represented as follows.

$$\begin{aligned} \dot{\mathbf{e}} &= \dot{\mathbf{x}} - \dot{\mathbf{x}}_d = \mathbf{A}\mathbf{x} + \mathbf{B}_1\delta_f + \mathbf{B}_2 u - \mathbf{A}_d\mathbf{x}_d - \mathbf{B}_d\delta_f \\ &= \mathbf{A}\mathbf{e} + (\mathbf{A} - \mathbf{A}_d)\mathbf{x}_d + (\mathbf{B}_1 - \mathbf{B}_d)\delta_f + \mathbf{B}_2 u \end{aligned} \tag{22}$$

Here, if the virtual input u^* is defined as follows $\boldsymbol{B}_2 u^* = (\boldsymbol{A} - \boldsymbol{A}_d)\mathbf{x}_d + (\boldsymbol{B}_1 - \boldsymbol{B}_d)\delta_f + \boldsymbol{B}_2 u$, then the (22) can be represented as (23).

$$\dot{\mathbf{e}} = \mathbf{A}\mathbf{e} + \mathbf{B}_2 u^* \tag{23}$$

The stability of the tracking error can be compensated by the feedback control law of $u^* = -\mathbf{K}\mathbf{e}$. Note that the error dynamic system written in (23) has the same matrix pair $(\mathbf{A}, \mathbf{B_2})$ as the zero-steering vehicle model to design the LQRs mentioned in Sections III-A through C. This means that the dynamic properties and parameter sensitivity of both systems are the same. Therefore, the previously obtained LQR gains, $\mathbf{K}_c$ and $\mathbf{K}_r$, can be equally applied to the virtual control input u^* as follows.

$$u^* = \begin{cases} -\mathbf{K}_c(\mathbf{x} - \mathbf{x}_d), \text{ for the conventional LQR} \\ -\mathbf{K}_r(\mathbf{x} - \mathbf{x}_d), \text{ for the robust LQR} \end{cases} \tag{24}$$

Finally, the actual control input for tracking the reference model can be obtained as follows.

$$u = M_z = \mathbf{B}_2^{\dagger}\left(\mathbf{B}_2 u^* - (\mathbf{A} - \mathbf{A}_d)\mathbf{x}_d - (\mathbf{B}_1 - \mathbf{B}_d)\delta_f\right) \tag{25}$$

After the desired yaw moment M_z is determined by the controllers, it should distribute the tire forces of each wheel. If the desired yaw moment is counterclockwise, the braking forces are exerted on the left tires. In the case of clockwise yaw moment, braking forces are exerted only on the right tires. Considering that the longitudinal acceleration affects the friction circle of the tire, the braking force is distributed to each wheel as (26). In (26), the subscripts *fl*, *fr*, *rl*, and *rr* represent the front left, front right, rear left, and rear right wheel, respectively.

$$\begin{aligned} M_z \geq 0 \quad \Rightarrow & \begin{cases} \Delta F_{x,fl} = \dfrac{2}{t_w}\dfrac{gl_{r,nom} - a_x h_{s,nom}}{gl} M_z \\ \Delta F_{x,rl} = \dfrac{2}{t_w}\dfrac{gl_{f,nom} + a_x h_{s,nom}}{gl} M_z \\ \Delta F_{x,fr} = 0 \\ \Delta F_{x,rr} = 0 \end{cases}, \\ M_z < 0 \quad \Rightarrow & \begin{cases} \Delta F_{x,fl} = 0 \\ \Delta F_{x,rl} = 0 \\ \Delta F_{x,fr} = -\dfrac{2}{t_w}\dfrac{gl_{r,nom} - a_x h_{s,nom}}{gl} M_z \\ \Delta F_{x,rr} = -\dfrac{2}{t_w}\dfrac{gl_{f,nom} + a_x h_{s,nom}}{gl} M_z \end{cases} \end{aligned} \tag{26}$$

IV. Simulation

To evaluate the performance of the proposed robust yaw stability controller, a simulation study that uses the commercial vehicle software Trucksim® and MATLAB/Simulink has been conducted. The driver model provided by Trucksim® is used for the simulation.

A. Simulation environment

Tire slip angle is an essential factor in evaluating the yaw stability of the vehicle. The linear tire model is valid at a slight tire slip angle, and the vehicle's behavior corresponds to its target behavior. As the tire slip angle increases, the difference between the vehicle's behavior and its target behavior increases due to the non-linear effect of the tire. In most cases, the large tire slip angles generate the yaw instability of the vehicle. Generally, the difference in slip angle between the front and rear wheels determine the cornering characteristics of the vehicle. The significant difference between front and rear wheels slip angle causes under-steer or over-steer conditions which are not desirable for the yaw stability of the vehicle.

Table II shows the three scenarios for evaluating the performance of the vehicle yaw stability controllers. Each scenario is characterized by three conditions, namely the driving, load, and road conditions.

TABLE II
SCENARIOS FOR EVALUATING THE VEHICLE YAW STABILITY CONTROL PERFORMANCE

Scenario	Driving condition	Load condition	Road condition
#1	J-Turn Const. Speed	Fully loaded	Low μ
#2	Double Lane Change Const. Speed	Rearward half loaded	Low μ
#3	Sine with Dwell Const. Speed	Fully loaded	Low μ

The first condition, i.e., driving, means maneuvering. The fast or excessive maneuvering results in large tire slip angles and huge slip angle differences between front and rear wheels. The second condition, i.e., load, means the weight of the load and the load distribution. Since the cornering stiffness could be approximated as parabolic about vertical tires, a vehicle with a heavy load requires larger tire slip angles than an empty vehicle when generating the same lateral acceleration. The load distribution causes the change of cornering characteristics. Generally, as the load is biased rearward of the vehicle, the vehicle has relatively over-steer characteristics.

The third condition, i.e., road, means a tire-road friction coefficient. At high μ, a commercial vehicle is more likely to encounter rollover before causing yaw instability because of its high center of gravity. At low μ, a vehicle has high probability of encountering yaw instability even at relatively small tire slip angle.

The proposed three scenarios incur the vehicle yaw instability situations, which can make a chance to evaluate the yaw stability controller. In scenario #1, the vehicle requires large tire slip angles to track the desired path, which

generates the vehicle's yaw instability. To initiate larger tire slip angles, the fully loaded condition is set. In scenario #2, an over-steer situation is initiated due to fast maneuvering, generating vehicle yaw instability. To emphasize the over-steer situation, the rearward half loaded condition is set. In scenario #3, large tire slip angles and over-steer situations are initiated. Several sine with dwell simulation studies found that the fully loaded condition generates the severest vehicle yaw instability. In all three scenarios, the low μ condition is set to make the severe vehicle yaw instability.

B. Scenario #1: J-turn

In scenario #1, J-turn cornering was conducted. Figure 10-(a) shows the steering input. The simulation assumed the vehicle was fully loaded (3000 kg) at the low μ condition. The tire-road friction coefficient was set to 0.5. The initial velocity of the vehicle was set to 75 km/h.

In Figures 10, 11, and 12, the legends CLQR and RLQR represent the conventional and robust LQR, respectively. In Figures 10-(g), (h), (i), 10-(g), (h), (i), and 12-(g), (h), (i) the titles FL, FR, RL, and RR represent the front left, front right, rear left, and rear right wheels, respectively.

Figure 10 provides the simulation results for scenario #1. In this simulation, the uncontrolled vehicle lost its yaw stability entirely due to low μ condition as shown in Figures 10-(c) and (e). Figure 10-(d) shows a strong induced over-steer of the uncontrolled vehicle. On the other hand, both the conventional and robust LQR controllers made the vehicle stable. While both controllers made the vehicle stable, the control performance of the RLQR, i.e., the yaw rate error and the side slip angle were superior to those of the CLQR as shown in Figures 10-(c), and (e). The RLQR applied more significant braking input than the CLQR from 2.5 to 4.4 s although the yaw rate error of the RLQR case is smaller than that of the CLQR case, as shown in Figures 10-(c) and (g). This is because the robust feedback gain $\mathbf{K}_r$ is designed to be greater than $\mathbf{K}_c$ to reduce parameter sensitivity. In this simulation, the vehicle has relatively close poles to the $j\omega$-axis on the s-plane due to small C_f and C_r caused by large tire slip angles and low μ. In this situation, the RLQR has higher yaw stability control performance than the CLQR because the RLQR secures more relatively stable poles than CLQR as shown in Figure 9. The CLQR applied more significant braking than the RLQR due to a much larger yaw rate error from 4.4 to 6.9 s as shown in Figures 10-(c), (g), and (h). Consequently, the CLQR decreased the longitudinal speed more compared to RLQR, as shown in Figure 10-(f). The vehicle with the RLQR had the most extended turning radius, indicating that the relatively slightest over-steer occurred. Consequently, a minor lateral tire force was imposed on the vehicle controlled by the RLQR, as shown in Figure 10-(i).

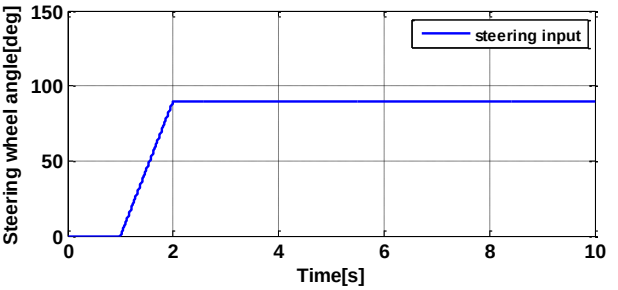

(a) Steering input

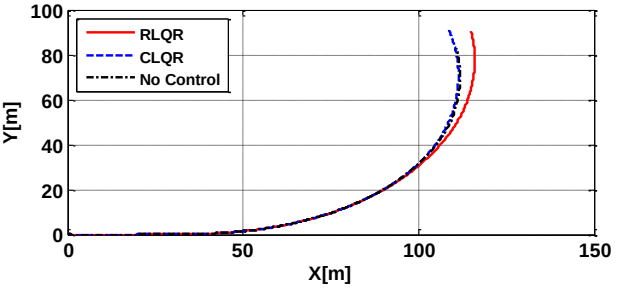

(b) Vehicle trajectory

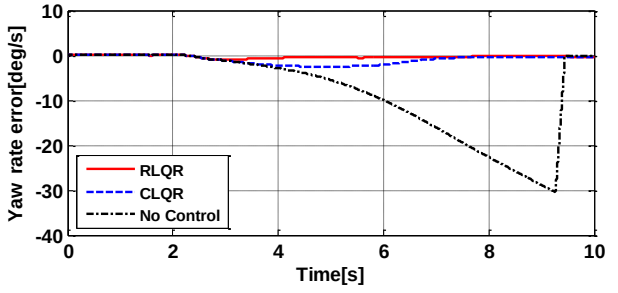

(c) Yaw rate error

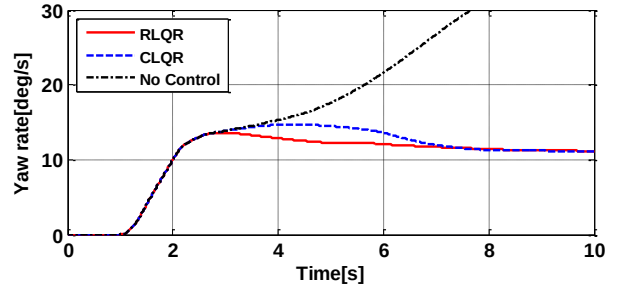

(d) Yaw rate

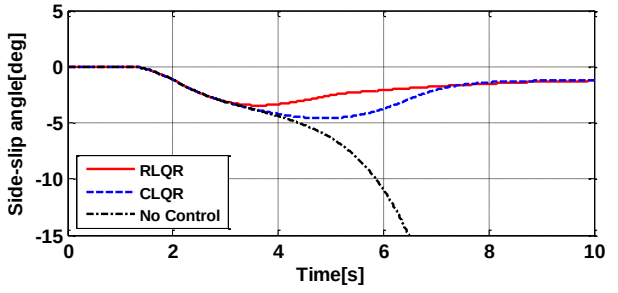

(e) Side-slip angle

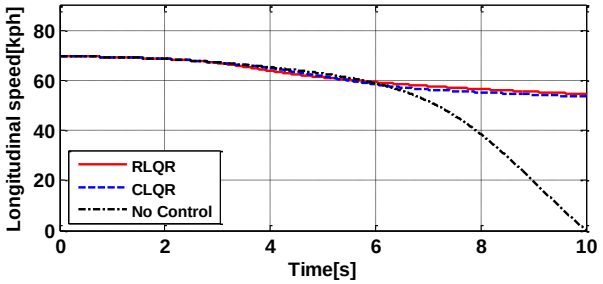

(f) Longitudinal speed

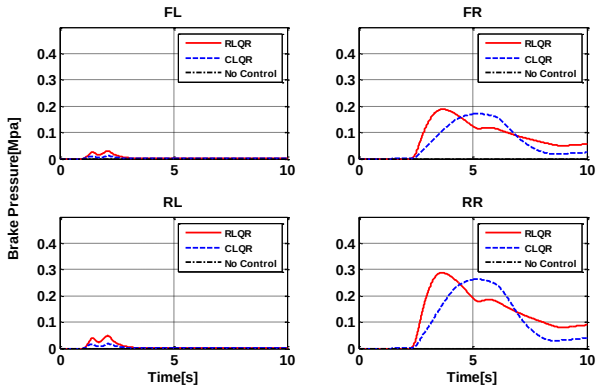

(g) Brake pressure

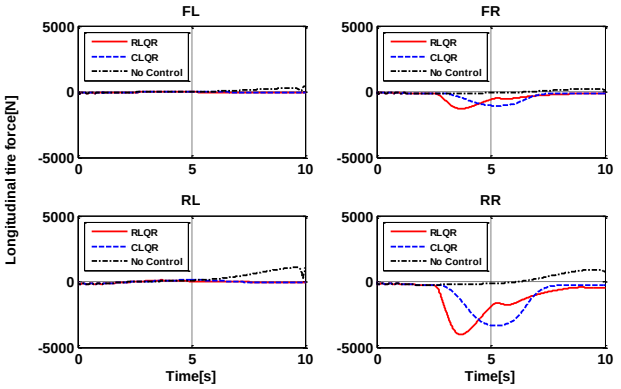

(h) Longitudinal tire force

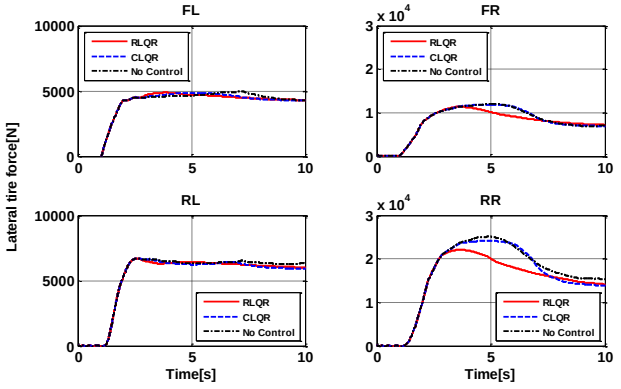

(i) Lateral tire force

FIGURE 10. Results of J-turn

C. Scenario #2: Double lane change

Scenario #2 conducts the double lane change. Figure 11-(a) shows the desired path. The simulation assumes that half of the limit load (1,500 kg) loads on the vehicle's rear at the low μ condition. The weight distribution, l_f, is 0.43 m larger than its nominal value. The tire-road friction coefficient was set to 0.5. The initial velocity of the vehicle was set to 100 km/h.

Figure 11 provides the simulation results of scenario # 2. In this simulation, the uncontrolled vehicle cannot track the desired path, as shown in Figure 11-(a). The driver model in the uncontrolled vehicle applied excessive steering input to reduce the position error. Nonetheless, the vehicle lost its yaw stability entirely due to low μ condition, as shown in Figures 11-(b), (c), (d), and (e). On the other hand, both the CLQR and RLQR made the vehicle stable for the double lane change. The control performance of the RLQR were superior to those of the CLQR, as shown in Figures 11-(b) and (e). The driver model with the RLQR applied less steering effort than the driver model with the CLQR due to higher yaw stability control performance of RLQR, as shown in Figure 11-(d). The RLQR applied more significant braking input than the CLQR from 2 to 6 s, although the yaw rate error of the RLQR case is smaller than that of the CLQR case, as shown in Figures 11-(b), (g), and (h). In this simulation, the vehicle has relatively close poles to the $j\omega$-axis on the s-plane due to relatively large value of $(l_fC_f - l_rC_r)/C_fC_r$, i.e., over-steering gradient, caused by the rearward loaded condition and low μ. Due to more significant braking input, the longitudinal speed of the vehicle with the RLQR decreased more than that of the vehicle with the CLQR until the simulation time was about 6 s, as shown in Figure 11-(f). This is expected from the fact that, in general, a robust controller gives a more significant control input than a nominal one [17]. The vehicle controlled by the RLQR had the slightest over-steer characteristics from 6 to 8 s, as shown in Figures 11-(c) and (e). Consequently, a minor lateral tire force is imposed on the vehicle controlled by the RLQR from 6 to 8 s, as shown in Figure 11-(i).

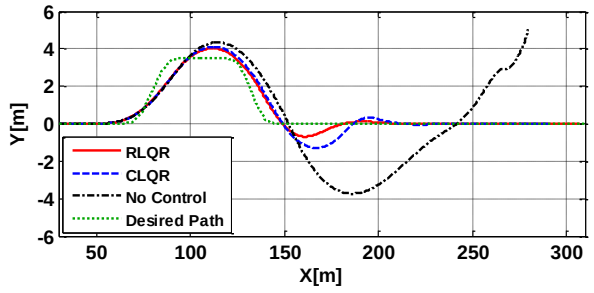

(a) Vehicle trajectory

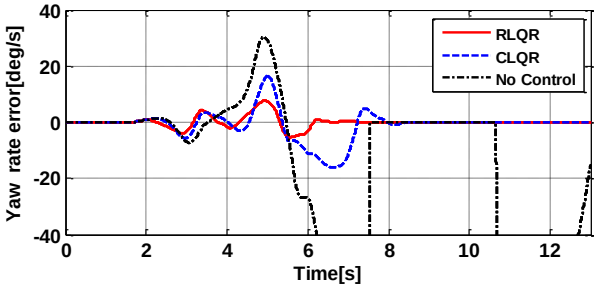

(b) Yaw rate error

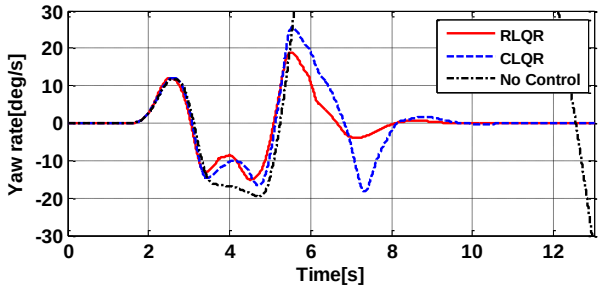

(c) Yaw rate

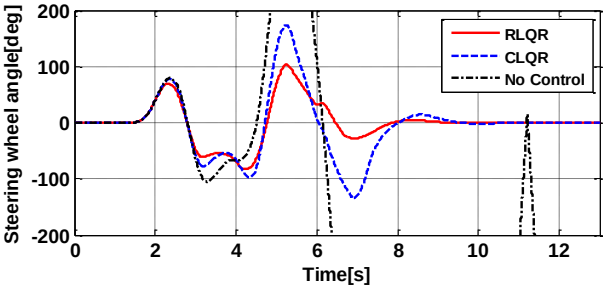

(d) Steering wheel angle

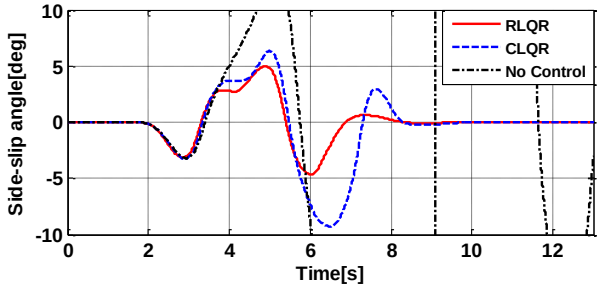

(e) Side-slip angle

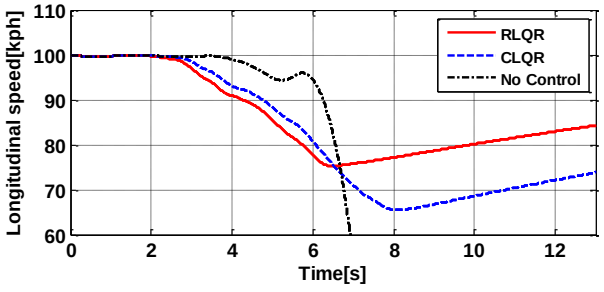

(f) Longitudinal speed

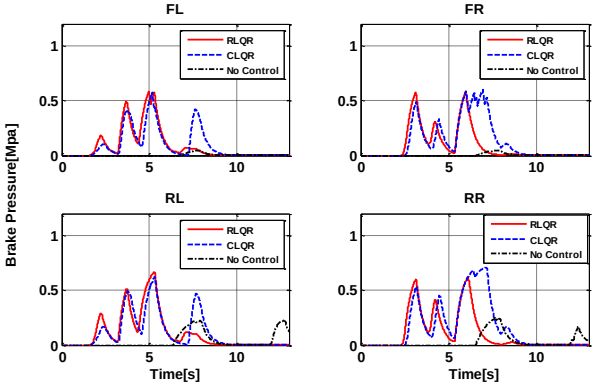

(g) Brake pressure

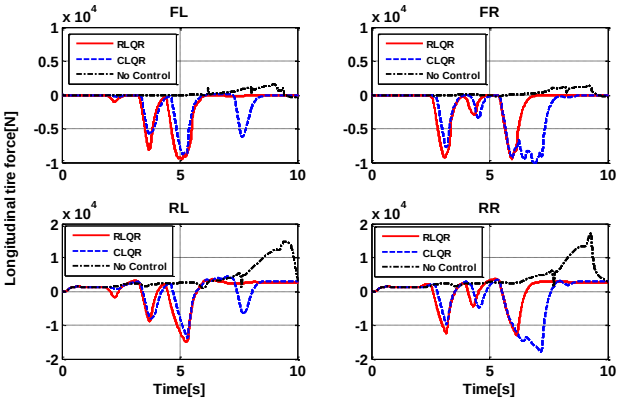

(h) Longitudinal tire force

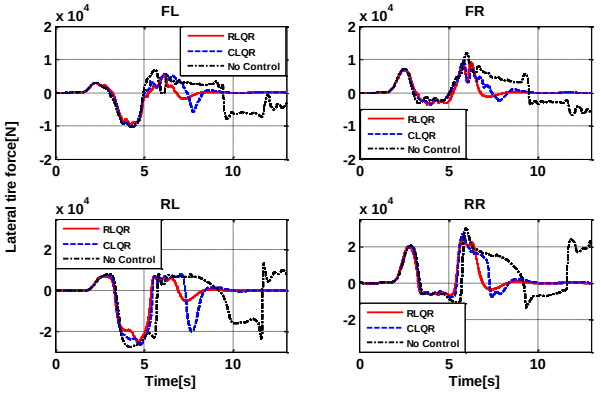

(i) Lateral tire force

FIGURE 11. Results of double lane change.

D. Scenario #3: Sine with dwell

In scenario #3, sine with dwell test was conducted. The sine with dwell steering input is shown in Figure 12-(a). In the simulation, it was assumed that that the vehicle is fully loaded (3000 kg) at the low μ condition. The tire-road friction coefficient was set to 0.5. The initial velocity of the vehicle was set to 75 km/h.

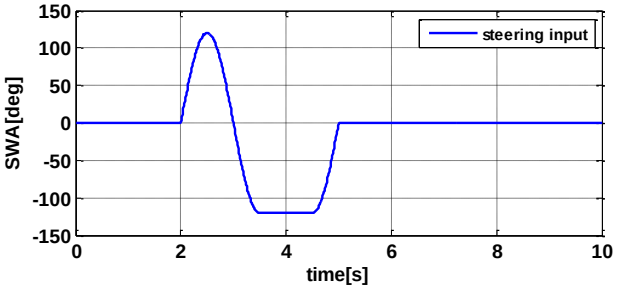

(a) Steering input

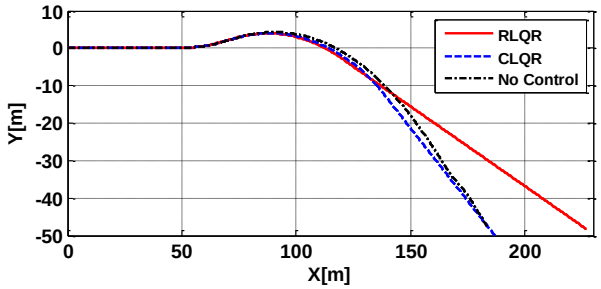

(b) Vehicle trajectory

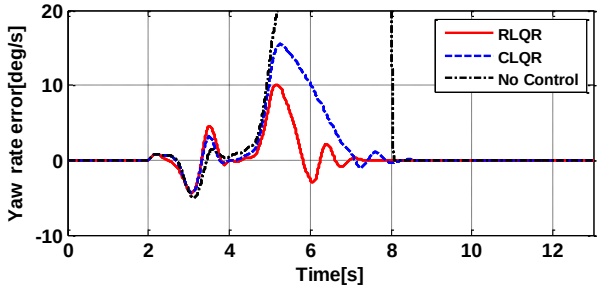

(c) Yaw rate error

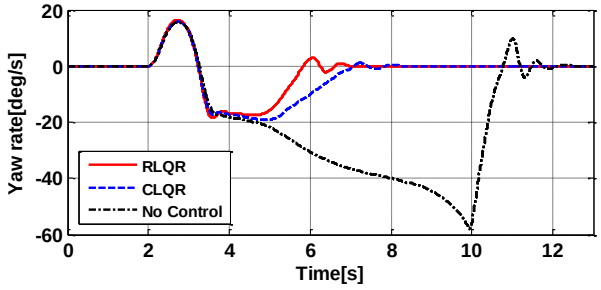

(d) Yaw rate

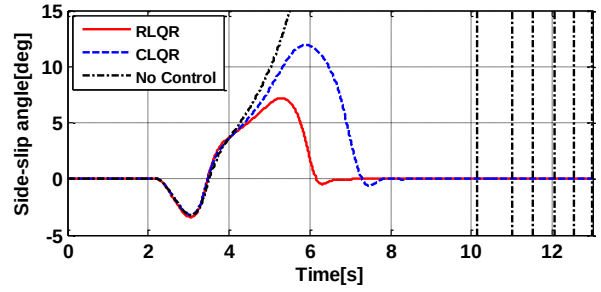

(e) Side-slip angle

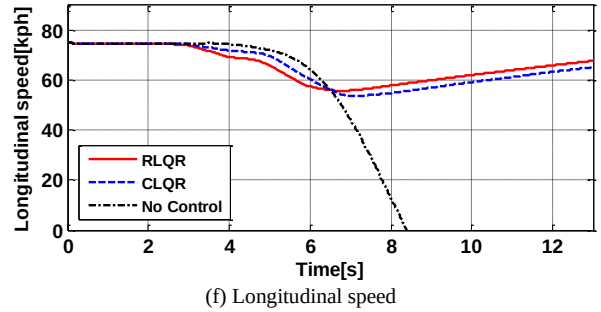

(f) Longitudinal speed

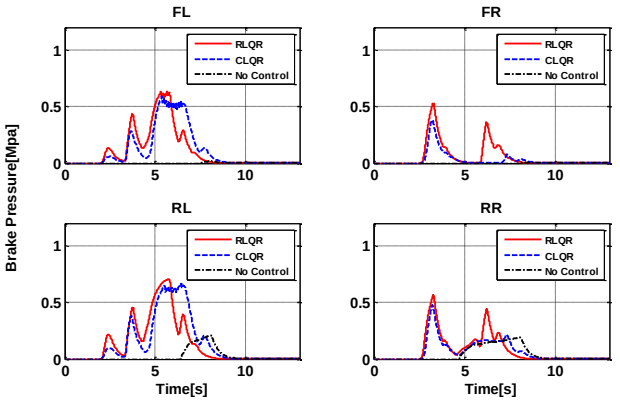

(g) Brake pressure

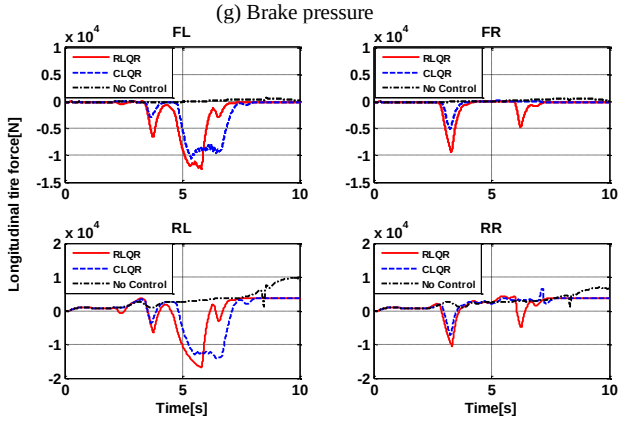

(h) Longitudinal tire force

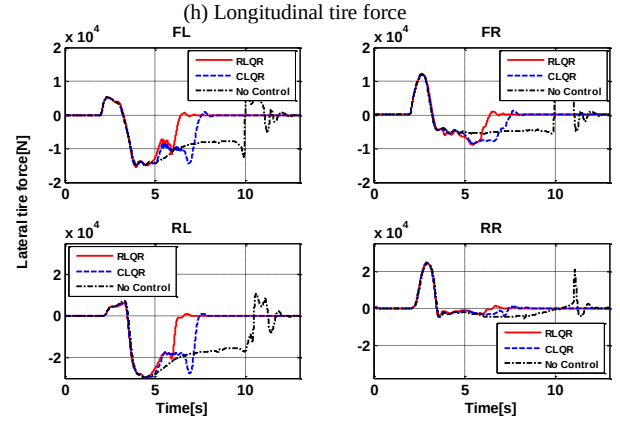

(i) Lateral tire force

FIGURE 12. Results of sine with dwell test.

Figure 12 shows the simulation results of scenario #3. In this simulation, the uncontrolled vehicle lost its yaw stability entirely after the steering input was completed due to low μ condition, as shown in Figures 12-(c), (d), and (e). On the other hand, both the conventional and robust LQR controllers made the vehicle stable. The control performances of RLQR are superior to those of the CLQR, as shown in Figures 12-(c), (d), and (e). The yaw rate of vehicle with RLQR converges to zero faster than that of the vehicle with CLQR after completing the steering input. In this simulation, the vehicle has poles relatively close to the $j\omega$-axis in the s-plane due to the small C_f and C_r caused by the large tire slip angles and low μ. The vehicle controlled by

the RLQR had the slightest over-steer characteristics from 5 to 8 s as shown in Figures 12-(d) and (e). The braking forces and the resulting vehicle speed tend to be like the ones in other scenarios.

E. Control performance analysis with respect to parameter variation

The second simulation analyzes the robust performance with load condition (load weight and load distribution) and road condition (tire-road friction coefficient). The simulation assumes that the distance from CG for the front axle, l_f, varies from 2.51 to 3.37 m, as the position of the half-loaded weight shifts from the front to the rear of the vehicle. The simulation also assumes that the sprung mass varies from 6360 to 9360 kg as the weight of the load transitions from minimum (0 kg) to maximum (3000 kg). The value of μ was set to 0.5 (low) and 0.85 (nominal).

Figures 13 and 14 show the root mean square (RMS) value of the yaw rate error and side-slip angle error for the CLQR and RLQR according to changes in load and road conditions.

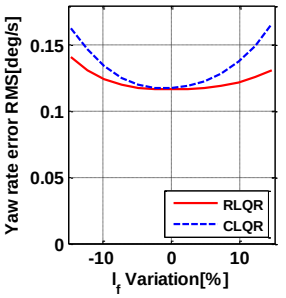

(a) RMS of yaw rate error with respect to l_f at μ of 0.85

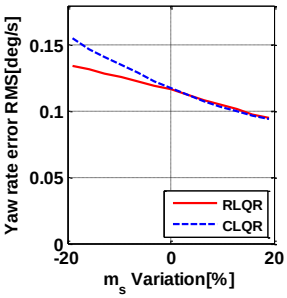

(b) RMS of yaw rate error with respect to m_s at μ of 0.85

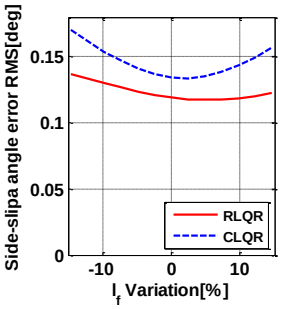

(c) RMS of side-slip angle error with respect to l_f at μ of 0.85

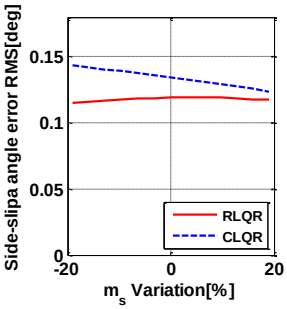

(d) RMS of side-slip angle error with respect to m_s at μ of 0.85

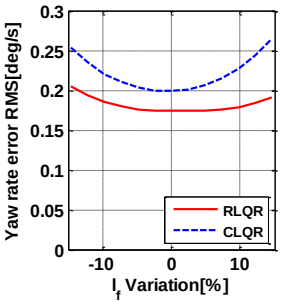

(e) RMS of yaw rate error with respect to l_f at μ of 0.5

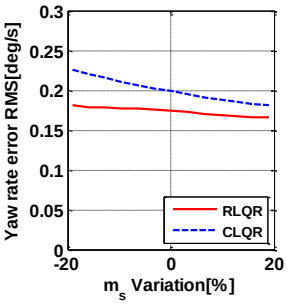

(f) RMS of yaw rate error with respect to m_s at μ of 0.5

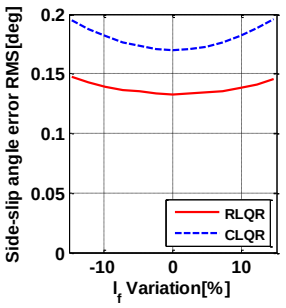

(g) RMS of side-slip angle error with respect to l_f at μ of 0.5

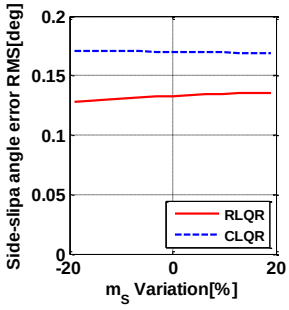

(h) RMS of side-slip angle error with respect to m_s at μ of 0.5

FIGURE 13. RMS of yaw rate and side-slip angle error with respect to variation of parameters for double lane change.

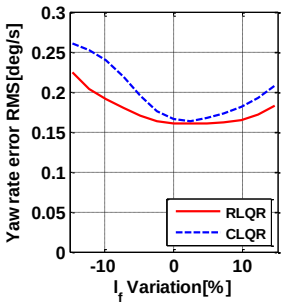

(a) RMS of yaw rate error with respect to l_f at μ of 0.85

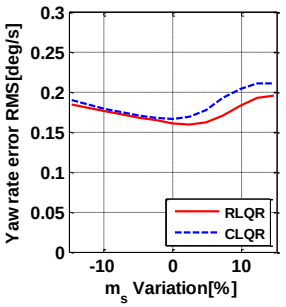

(b) RMS of yaw rate error with respect to m_s at μ of 0.85

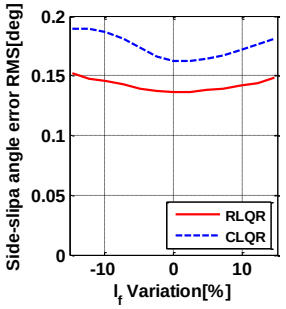

(c) RMS of side-slip angle error with respect to l_f at μ of 0.85

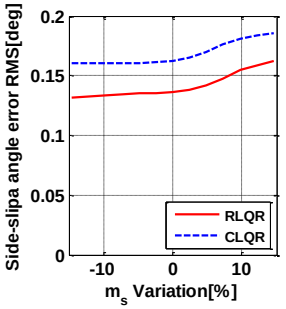

(d) RMS of side-slip angle error with respect to m_s at μ of 0.85

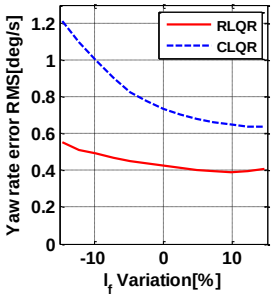

(e) RMS of yaw rate error with respect to l_f at μ of 0.5

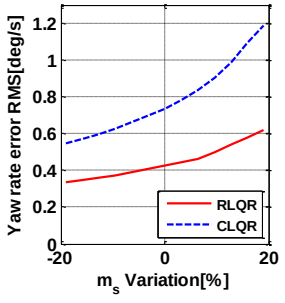

(f) RMS of yaw rate error with respect to m_s at μ of 0.5

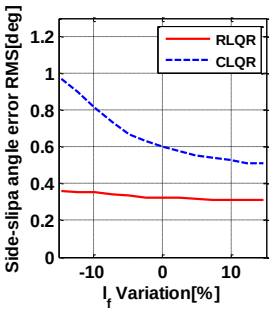

(g) RMS of side-slip angle error with respect to l_f at μ of 0.5

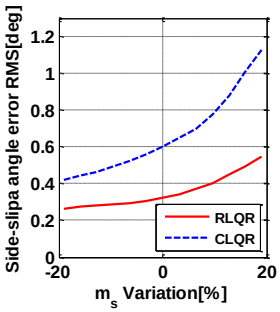

(h) RMS of side-slip angle error with respect to m_s at μ of 0.5

FIGURE 14. RMS of yaw rate and side-slip angle error with respect to variation of parameters for sine with dwell test.

Figure 13 shows the results of the double lane change scenario, and Figure 14 shows the results of the sine with dwell test scenario. These results show that the performance of the RLQR is less sensitive to parameter changes in commercial vehicle than that of the CLQR. As shown in Figures 13-(a), (b), (c), (d), 13-(a), (b), (c), and (d), the performance of the CLQR is as good as the RLQR at nominal vehicle parameters and μ condition. However, the performance variation of the RLQR is smaller than that of the CLQR. As shown in Figures 13-(e), (f), (g), (h), 14-(e), (f), (g), and (h), in the case of low μ, the performance of RLQR is better than the CLQR even at nominal vehicle parameter. Moreover, the performance variation of the RLQR is much smaller than that of the CLQR. These results indicate that the proposed RLQR is more effective for yaw stability control against the parameter uncertainties in commercial vehicles.

V. Conclusion

This paper proposed a robust yaw stability controller for commercial vehicles to reduce performance sensitivities due to the parameter variances. The conducted analysis obtains the stochastic root locus in the commercial vehicle parameters. The conventional LQR controller for yaw stability uses the nominal vehicle parameter design. Considering the parameter uncertainty, the parameter sensitivity reduction method was adopted to design the robust controller. The parameter sensitivity analysis of commercial vehicles showed that the variation of cornering stiffness and the distance from C.G. to the front axle have a relatively significant effect on the state trajectory. The LQ cost function was modified to reduce the parameter sensitivity of the state trajectory. To determine the optimal gain of the robust controller, minimizing the area and variance of the stochastic root locus was considered through Monte Carlo run. The robust LQR is expected to perform insensitively against the parameter variation in the sense of stochastic root locus. The proposed controller was designed with the linear vehicle model and applied to the non-linear vehicle model in Trucksim®. A simulation study has been conducted to evaluate the proposed controller. The scenarios assumed severe maneuvering, loading, and low-friction roads to show the difference in performance between the conventional LQR and the robust one. The simulation results show that although the performance of the conventional LQR is as good as that of the robust one at nominal vehicle parameters and under nominal road condition, the performance variation of the robust LQR is less sensitive to parameter variations than that of the conventional one.

If the tire force, tire-slip angle, tire characteristics, tire-road friction coefficient, etc., can be estimated accurately, non-linear control strategies such as a gain-scheduled control and an adaptive control could be alternatives to the robust control in future work.

REFERENCES

[1] National Highway Traffic Safety Administration, "FMVSS No. 136 - Electronic Stability Control Systems on Heavy Vehicles," June 2014.
[2] National Highway Traffic Safety Administration, "Heavy Truck ESC Effectiveness Study Using NADS – Final Report," November 2009.
[3] L. Güvenç, Ş.S. Ersolmaz, S. Öncü, E.S. Öztürk, E. Çetin, N. Klç, S. Güngör, and A. Kanbolat, "Stability enhancement of a light commercial vehicle using active steering," SAE Technical Paper 2006-01-1181, 2006.
[4] B. Zheng, S. Anwar, "Yaw stability control of a steer-by-wire equipped vehicle via active front wheel steering," Mechatronics, Vol. 19, No. 6, 2009, pp. 799-804.
[5] B.L. Boada, M.J.L. Boada, and V. Diaz, "Fuzzy-logic applied to yaw moment control for vehicle stability," Vehicle System Dynamics, Vol. 43, No. 10, 2005, pp. 753-770.
[6] E. Esmailzadeh, A. Goodarzi, and G.R. Vossoughi, "Optimal yaw moment control law for improved vehicle handling," Mechatronics, Vol. 13, No.7, 2003, pp. 659-675.
[7] C. Zhao, W. Xiang, and P. Richardson, "Vehicle lateral control and yaw stability control through differential braking," IEEE Industrial Electronics Symposium, 2006, Montreal, Canada.
[8] S. Zhang, T. Zhang, and S. Zhou, "Vehicle stability control strategy based on active torque distribution and differential braking," IEEE Measuring Technology and Mechatronics Automation Conference, 2009, Zhangjiajie, China.
[9] B.A. Guvenc, T. Acarman, and L. Guvenc, "Coordination of steering and individual wheel braking actuated vehicle yaw stability control," Proceedings of the IEEE Intelligent Vehicles Symposium, 2003, pp. 288-293.
[10] S.D. Cairano, H.E. Tseng, D. Bernardini, and A. Bemporad, "Vehicle yaw stability control by coordinated active front steering and differential braking in the tire sideslip angles domain," IEEE Transactions on Control Systems Technology, Vol. 21, No. 4, 2013, pp. 1236-1248.
[11] C. Chen, M. Tomizuka, "Lateral Control of Commercial Heavy Vehicles," Vehicle System Dynamics, Vol. 33, No. 6, 2000, pp. 391-420.
[12] P. Sun, A. S. Trigell, L. Drugge, and J. Jerrelind, "Energy efficiency and stability of electric vehicles utilising direct yaw moment control," Vehicle system dynamics, Vol.60, No.3, 2022, pp. 930-950.
[13] X. Hu, H. Chen, Q. Ren, X. Gong, P. Wang, and Y. Hu, "Estimation and Expansion of Vehicle Stability Region With Sums of Squares Programming," IEEE/ASME Transactions on Mechatronics, Vol. 28, No.5, 2023, pp. 2820-2831.
[14] X. Hu, P. Wang, S. Cai, L. Zhang, Y. Hu, and H. Chen, "Vehicle stability analysis by zero dynamics to improve control performance," IEEE Transactions on Control Systems Technology, Vol. 31, No. 6, 2023, pp. 2365-2379.
[15] M. Ploechl, P. Lugner, and A. Riepl., "Improvements of passenger car-trailer behaviour by a trailer based control system," Vehicle System Dynamics, Vol. 29, Supplement 1, 1998, pp. 438-450.

[16] S. Oncu, S. Karaman, L. Guvenc, S.S. Ersolmaz, E.S. Ozturk, E. Cetin and M. Sinal, “Robust Yaw Stability Controller Design for a Light Commercial Vehicle Using a Hardware in the Loop Steering Test Rig,” IEEE Intelligent Vehicles Symposium, 2007, Istanbul, Turkey.
[17] S. Yim, Y. Park, “Design of Rollover Prevention Controller with Linear Matrix Inequality-based Trajectory Sensitivity Minimisation,” Vehicle System Dynamics, Vol. 49, No. 8, 2011, pp. 1225-1244.
[18] S. Yim, “Design of a Robust Controller for Rollover Prevention with Active Suspension and Differential Braking,” Journal of Mechanical Science and Technology, Vol. 26, No.1, 2011, pp. 1-10.
[19] L. Palkovics, M. El-Gindy. “Design of an active unilateral brake control system for five-axle tractor-semitrailer based on sensitivity analysis,” Vehicle System Dynamics, Vol. 24, No.10, 1995, pp. 725-758.
[20] A.J. Calise, E.V. Byrns Jr., “Parameter Sensitivity Reduction in Fixed-Order Dynamic Compensation,” Journal of Guidance, Control, and Dynamics, Vol. 15, No. 2, 1992, pp. 440-447.
[21] R.F. Stengel, L.R. Ray, “Stochastic Robustness of Linear Time-Invariant Control Systems,” IEEE Transactions on Automatic Control, Vol. 36, No. 1, 1991, pp. 82-87.
[22] Q. Wang, R.F. Stengel, “Robust Control of Nonlinear Systems with Parametric Uncertainty,” Proceedings of the 37th IEEE Conference on Decision & Control, Tampa, Florida, USA, December 1998.
[23] B. Kwon, S. Kim, and K. Yi, “Design of a robust yaw stability controller for commercial vehicles with parameter sensitivity reduction and stochastic root locus,” IEEE Intelligent Vehicles Symposium, 2015, Seoul, South Korea.
[24] D.D. Moerder, A.J. Calise, “Convergence of a Numerical Algorithm for Calculating Optimal Output Feedback Gains,” IEEE Transactions on Automatic Control, Vol. 30, No. 9, 1985, pp. 900-903.
[25] J. Yoon, W. Cho, B. Koo, and K. Yi, “Unified chassis control for rollover prevention and lateral stability,” IEEE Transactions on Vehicular Technology, Vol. 58, No. 2, 2009, pp. 596-609.
[26] M. Nagai, Y. Hirano, and S. Yamanaka, "Integrated control of active rear wheel steering and direct yaw moment control," Vehicle System Dynamics, Vol. 27, No.5-6, 1997, pp. 357-370.

Jae-Hoon Jeong received the B.S., M.S., and Ph.D. degrees in Control and Instrumentation Engineering from Pukyong National University, Busan, Republic of Korea in 2015, 2017, and 2020, respectively.

In 2020, he was a Senior Researcher with the Korea Railroad Research Institute. Since 2021, he has been an Assistant Professor with Kunsan National University. His research interests include signal processing, embedded system design, sensor networks, digital control, artificial intelligence systems, and light rail transit.

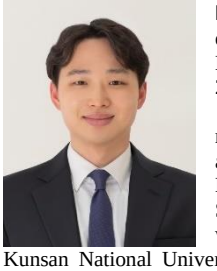

Baek-soon Kwon received the B.S. and Ph.D. degrees in Mechanical Engineering from Seoul National University, Seoul, Republic of Korea in 2013 and 2018, respectively.

From 2018 to 2020, he was a postdoctoral researcher at Seoul National University. He served as a staff engineer at Samsung Electronics, Mechatronics R&D Center, from 2020 to 2021. Since 2021, he has been an Assistant Professor with the Mechanical Engineering Department, Kunsan National University. His research interests include autonomous driving, vehicle active safety, vehicle suspension control, and fault-tolerant systems.